Large-Scale Characteristic Mode Analysis With Fast Multipole Algorithms

Qi I. Dai, *Member, IEEE*, Junwei Wu, Hui Gan, *Student Member, IEEE*, Qin S. Liu, *Student Member, IEEE*, Weng Cho Chew, *Fellow, IEEE*, and Wei E. I. Sha, *Member, IEEE*

***Abstract*—Large-scale characteristic mode analysis (CMA) poses challenges in computational electromagnetics as it calls for efficient solutions of large dense generalized eigenvalue problems. In this paper, we consider two applications that involve large-scale CMA, and demonstrate that fast multipole algorithms (FMAs) can be easily incorporated into the implicitly restarted Arnoldi method (IRAM) for eigenanalysis after simple modifications. The first application performs CMA for large platforms made by closed perfectly conducting surfaces. Multilevel FMA (MLFMA) is embedded into a combined field integral equation-based theory of characteristic mode (TCM). The second application addresses multiscale modeling of small but geometrically complicated objects, which possess fine subwavelength structures. An augmented electric field integral equation-based TCM is formulated, and low-frequency (LF-)FMA is adopted to accelerate the required matrix–vector products.**

***Index Terms*—Augmented electric field integral equation, characteristic mode, combined field integral equation, fast multipole algorithm (FMA), large scale.**

I. Introduction

AFTER its humble beginnings in the 1970s, characteristic mode analysis (CMA) has gained a recent resurgence of interest in the field of antenna design and optimization. Initiated by Garbacz and refined by Harrington and Mautz [1]–[3], CMA was popularized in the antenna community by the work of Cabedo–Fabrés, as it has been shown promising for systematic antenna design [4]. Such a systematic approach becomes increasingly favored, since heuristic approaches based on the experience and intuition of antenna engineers hardly survive the demanding requirement of designing complex antenna systems. CMA is capable of characterizing an arbitrary object's radiation and scattering properties only relying on its geometry and material properties rather than the source configuration, which makes it a favorable candidate for systematic design methods where complicated functionality tradeoffs can be handled. Moreover, CMA provides useful physical insight into antenna operation as well as guidance on the excitation of desired radiating modes [5]–[7].

Although CMA has shown success in antenna design and synthesis, a relatively little effort has been devoted to characteristic mode computation. Development of new theory of characteristic mode (TCM) becomes indispensable in various large-scale applications where the conventional theory based on an electric field integral equation (EFIE) fails to properly function. One example is an automotive antenna where a coupling element excites multimodes of a large platform (closed vehicle chassis), and the entire platform operates as an antenna [8]. In this case, the conventional theory suffers from the spurious internal resonance corruption [9]. Another example is multiscale modeling of a small complex geometry, such as a metamaterial-inspired antenna. Due to the existence of fine subwavelength structures, a portion or all of the mesh elements are of small electrical size, which normally results in a large number of unknowns. In this case, the conventional theory may be susceptible to a low frequency or dense mesh breakdown [10].

Regarding computational complexity, current strategies of CMA can only deal with small-scale problems as they explicitly generate EFIE impedance matrices. The memory cost is $O(N^2)$, where N is the number of unknowns resulted from the method of moment (MoM). The complexity of computing all eigenpairs (eigenvalues and eigenvectors) of a dense generalized eigenvalue problem is $O(N^3)$ with QZ factorization. Normally, it is not the entire eigenspectrum that is of interest. The desired spectral portion, i.e., small eigenvalues, corresponds to efficient radiating modes that dominate the induced current excited by an arbitrary source [4], [11]. This portion can be iteratively solved for using Krylov subspace methods such as Lanczos or Arnoldi algorithms [12]–[14]. A number of matrix vector products (MVPs) are performed in such methods, each of which has a computational complexity of $O(N^2)$. Even so, this $O(N^2)$ complexity hinders large-scale CMA in the aforementioned applications.

It is well known that fast multipole algorithms (FMAs) can be used to accelerate MVPs in large-scale EM scattering problems, among which the multilevel version based on translation, interpolation, anterpolation, and a grid-tree structure greatly reduces both computational and memory costs of MVPs to $O(N \log N)$ [15]–[19]. In this paper, we address large-scale CMA by embedding FMAs into iterative eigensolvers such as the implicitly restarted Arnoldi method (IRAM) [12], [13]

Manuscript received November 21, 2014; revised October 31, 2015; accepted January 15, 2016. Date of publication February 05, 2016; date of current version July 04, 2016. This work was supported in part by the National Science Foundation under Award number 1218552, in part by the Research Grants Council of Hong Kong under Grant GRF 711609 and Grant 711508, and in part by the University Grants Council of Hong Kong (Contract AoE/P-04/08).

Q. I. Dai, H. Gan, and W. C. Chew are with the Department of Electrical and Computer Engineering, University of Illinois at Urbana-Champaign, Urbana, IL 61801 USA (e-mail: daiqi@illinois.edu; huigan2@illinois.edu; w-chew@uiuc.edu).

J. Wu is with the School of Electronics and Information, Wuhan University, Hubei 430072, China (e-mail: jun_wei_wu@yahoo.com).

Q. S. Liu and W. E. I. Sha are with the Department of Electrical and Electronic Engineering, University of Hong Kong, Pokfulam, Hong Kong (e-mail: qinliu@eee.hku.hk; wsha@eee.hku.hk).

Color versions of one or more of the figures in this paper are available online at http://ieeexplore.ieee.org.

Digital Object Identifier 10.1109/TAP.2016.2526083

and/or the Jacobi–Davidson QZ (JDQZ) method [14]. To analyze a large closed platform, a combined-field integral equation (CFIE)-based TCM is employed to remove the spurious internal resonance corruption. Multilevel FMA (MLFMA) is modified to accelerate the required MVPs. On the other hand, to remedy the difficulty in multiscale modeling of small complex geometries, we reformulate TCM on the top of an augmented electric field integral equation (A-EFIE) [10], and accelerate the required MVPs with a low-frequency (LF-) FMA [20]. Numerical examples are presented to validate and demonstrate the performance of the proposed schemes. This work paves the way of CMA for large-scale and complicated 3-D objects with limited computational resources.

II. TCM Based on EFIE

As suggested by Harrington and Mautz [3], the characteristic mode theory for an arbitrarily shaped perfectly conducting surface S is formulated on top of EFIE as

$$\mathcal{X}_E(\mathbf{r},\mathbf{r}')\cdot\mathbf{J}_n(\mathbf{r}')=\lambda_n\mathcal{R}_E(\mathbf{r},\mathbf{r}')\cdot\mathbf{J}_n(\mathbf{r}')\quad \mathbf{r}\in S \tag{1}$$

where λ_n and $\mathbf{J}_n$ correspond to the characteristic values and currents, respectively. Note that integration is implied over repeated variables in this paper. The real and imaginary parts of the EFIE impedance operator $\mathcal{Z}_E$ are denoted by $\mathcal{R}_E$ and $\mathcal{X}_E$, respectively. The impedance operator applies to a surface current as

$$\mathcal{Z}_E(\mathbf{r},\mathbf{r}')\cdot\mathbf{J}(\mathbf{r}')=-\bar{\mathbf{I}}_t\cdot ik\eta\int_S d\mathbf{r}'\overline{\mathbf{G}}(\mathbf{r},\mathbf{r}')\cdot\mathbf{J}(\mathbf{r}') \tag{2}$$

where k is the wavenumber, $\eta=\sqrt{\mu/\varepsilon}$ is the characteristic impedance of free space, and $\bar{\mathbf{I}}_t=\bar{\mathbf{I}}-\hat{n}\hat{n}$ extracts the tangential components of the field with $\bar{\mathbf{I}}$ denoting a unit dyad, $\hat{n}$ the unit normal of the surface. In the above, and Green's dyad is

$$\overline{\mathbf{G}}(\mathbf{r},\mathbf{r}')=\left[\bar{\mathbf{I}}-\frac{\nabla\nabla'}{k^2}\right]g(\mathbf{r},\mathbf{r}') \tag{3}$$

with

$$g(\mathbf{r},\mathbf{r}')=\frac{e^{ikR}}{R}\quad R=|\mathbf{r}-\mathbf{r}'|. \tag{4}$$

Approximating the surface current $\mathbf{J}(\mathbf{r})$ with Rao–Wilton–Glisson (RWG) basis functions $\mathbf{f}_j(\mathbf{r})$, we obtain the matrix representation of $\mathcal{Z}_E$ as

$$[Z_E]_{ij}=-ik\eta\int_s d\mathbf{r}\,\mathbf{f}_i(\mathbf{r})\cdot\int_s\overline{\mathbf{G}}(\mathbf{r},\mathbf{r}')\cdot\mathbf{f}_j(\mathbf{r}')\,d\mathbf{r}' \tag{5}$$

with Galerkin's procedure where testing functions are chosen to be the same as basis functions. Equation (1), therefore, leads to a generalized eigenvalue problem as

$$\overline{\mathbf{X}}_E\cdot\mathbf{J}_n=\lambda_n\overline{\mathbf{R}}_E\cdot\mathbf{J}_n \tag{6}$$

where the resistance and reactance matrices $\overline{\mathbf{R}}_E$ and $\overline{\mathbf{X}}_E$ correspond to the real and imaginary parts of the impedance matrix $\overline{\mathbf{Z}}_E$, respectively.

Usually, one can obtain good approximations to the eigenvalues with large magnitudes using Krylov subspace iterations [13]. It is hence straightforward, as suggested in the ARnoldi PACKage (ARPACK) [13], or implemented in the commercial suite FEKO [11], to convert (6) to a standard eigenvalue problem as

$$\overline{\mathbf{X}}_E^{-1}\cdot\overline{\mathbf{R}}_E\cdot\mathbf{J}_n=\lambda_n^{-1}\mathbf{J}_n \tag{7}$$

for fast convergence to desired eigenspectra (small eigenvalues), which correspond to efficient radiating modes. A number of MVPs in the form of $\overline{\mathbf{X}}_E^{-1}\cdot\mathbf{u}$ have to be computed, where $\mathbf{u}$ are the arbitrary vectors. If $\overline{\mathbf{X}}_E^{-1}\cdot\mathbf{u}$ is solved iteratively, it is favored to solve an equivalent eigenvalue problem given by

$$\overline{\mathbf{Z}}_E^{-1}\cdot\overline{\mathbf{R}}_E\cdot\mathbf{J}_n=(1+i\lambda_n)^{-1}\mathbf{J}_n \tag{8}$$

since efficient preconditioners exist for expediting iterative convergence to EFIE solutions $\overline{\mathbf{Z}}_E^{-1}\cdot\mathbf{u}$.

III. TCM Based on CFIE

Conventional EFIE-based TCM can hardly be used to solve for characteristic modes of large closed platforms, where $\overline{\mathbf{Z}}_E$ are ill-conditioned due to spurious internal resonances. In a recent paper, we formulated a CFIE-based TCM as [9], [21]

$$\begin{aligned}&[\alpha\mathcal{Z}_E(\mathbf{r},\mathbf{r}')+(1-\alpha)\eta\mathcal{Z}_H(\mathbf{r},\mathbf{r}')]\cdot\mathbf{J}_n(\mathbf{r}')\\&\quad=(1+i\lambda_n)\,[\alpha\mathcal{R}_E(\mathbf{r},\mathbf{r}')+(1-\alpha)i\eta\mathcal{X}_H(\mathbf{r},\mathbf{r}')]\cdot\mathbf{J}_n(\mathbf{r}')\end{aligned} \tag{9}$$

where $\mathbf{r}\in S$, α is the CFIE combination coefficient, and $\mathcal{X}_H$ is the imaginary part of the magnetic field integral operator $\mathcal{Z}_H$, which is given by

$$\begin{aligned}\mathcal{Z}_H(\mathbf{r},\mathbf{r}')\cdot\mathbf{J}(\mathbf{r}')=&2\pi\bar{\mathbf{I}}_t\cdot\mathbf{J}(\mathbf{r})-\bar{\mathbf{I}}_t\cdot\hat{n}\\&\times P.V.\int_S d\mathbf{r}'\nabla g(\mathbf{r},\mathbf{r}')\times\mathbf{J}(\mathbf{r}').\end{aligned} \tag{10}$$

After discretizing (9), one can obtain the matrix eigenvalue equation as

$$\overline{\mathbf{Z}}_C\cdot\mathbf{J}_n=(1+i\lambda_n)\overline{\mathbf{M}}_C\cdot\mathbf{J}_n \tag{11}$$

where

$$\overline{\mathbf{Z}}_C=\alpha\overline{\mathbf{Z}}_E+(1-\alpha)\eta\overline{\mathbf{Z}}_H \tag{12a}$$

$$\overline{\mathbf{M}}_C=\alpha\overline{\mathbf{R}}_E+(1-\alpha)i\eta\overline{\mathbf{X}}_H. \tag{12b}$$

In the above, $\overline{\mathbf{Z}}_E$ and $\overline{\mathbf{R}}_E$ have the same definition as before, while $\overline{\mathbf{Z}}_H$ and $\overline{\mathbf{X}}_H$ are the matrix representations of operators $\mathcal{Z}_H$ and $\mathcal{X}_H$, respectively. For simplicity, RWG functions are adopted herein to discretize the magnetic field integral operator, such that

$$\begin{aligned}[Z_H]_{ij}=&\,2\pi\int_s d\mathbf{r}\,\mathbf{f}_i(\mathbf{r})\cdot\mathbf{f}_j(\mathbf{r})\\&-\int_s d\mathbf{r}\,\mathbf{f}_i(\mathbf{r})\cdot\hat{n}\times\nabla\times\int_s g(\mathbf{r},\mathbf{r}')\mathbf{f}_j(\mathbf{r}')\,d\mathbf{r}'.\end{aligned} \tag{13}$$

Otherwise, Buffa–Christiansen (BC) or Chen–Wilton (CW) basis functions can be used as the testing functions for a better discretization accuracy [22]–[24]. Since $\overline{\mathbf{Z}}_C$ is full rank even at frequencies of internal resonances, we convert (11) to a standard eigenvalue equation as

$$\overline{\mathbf{Z}}_C^{-1} \cdot \overline{\mathbf{M}}_C \cdot \mathbf{J}_n = (1 + i\lambda_n)^{-1}\mathbf{J}_n \tag{14}$$

which can be easily solved using iterative methods.

IV. TCM Based on A-EFIE

In multiscale modeling, an electrically small object may result in a large number of unknowns due to the dense discretization on its fine subwavelength parts. This renders $\overline{\mathbf{Z}}_E$ ill-conditioned, and hinders solving $\overline{\mathbf{Z}}_E^{-1} \cdot \mathbf{u}$ iteratively. In excitation problems, this difficulty has been remedied with an augmented EFIE (A-EFIE) [10].

In light of the following decomposition:

$$\overline{\mathbf{Z}}_E = ik\eta\overline{\mathbf{V}} + \frac{\eta}{ik}\overline{\mathbf{D}}^T \cdot \overline{\mathbf{P}} \cdot \overline{\mathbf{D}} \tag{15}$$

with definitions of matrices $\overline{\mathbf{V}}$, $\overline{\mathbf{P}}$, and $\overline{\mathbf{D}}$ provided in [10], the EFIE-based TCM can be reformulated on top of A-EFIE as

$$\overline{\mathbf{Z}}_A \cdot \begin{bmatrix} ik\mathbf{J}_n \\ c\boldsymbol{\rho}_n \end{bmatrix} = (i - \lambda_n)\overline{\mathbf{X}}_A \cdot \begin{bmatrix} ik\mathbf{J}_n \\ c\boldsymbol{\rho}_n \end{bmatrix} \tag{16}$$

or

$$\overline{\mathbf{R}}_A \cdot \begin{bmatrix} ik\mathbf{J}_n \\ c\boldsymbol{\rho}_n \end{bmatrix} = -\lambda_n\overline{\mathbf{X}}_A \cdot \begin{bmatrix} ik\mathbf{J}_n \\ c\boldsymbol{\rho}_n \end{bmatrix} \tag{17}$$

where $c^{-1} = \sqrt{\mu\epsilon}$, and $\mathbf{J}_n$ and $\boldsymbol{\rho}_n$ are the characteristic currents and charges, respectively. By explicitly enforcing the charge neutrality condition, we have

$$\overline{\mathbf{Z}}_A = \begin{bmatrix} \overline{\mathbf{V}} & \overline{\mathbf{D}}^T \cdot \overline{\mathbf{P}} \cdot \overline{\mathbf{B}} \\ \overline{\mathbf{F}} \cdot \overline{\mathbf{D}} & k^2\overline{\mathbf{I}} \end{bmatrix} \tag{18}$$

where $\overline{\mathbf{F}}$ and $\overline{\mathbf{B}}$ are forward and backward mapping matrices between full and reduced charge vectors, respectively, and $\overline{\mathbf{I}}$ is an identity matrix of reduced dimension, as defined in [10]. Besides, $\overline{\mathbf{X}}_A$ and $\overline{\mathbf{R}}_A$ are the imaginary and real parts of $\overline{\mathbf{Z}}_A$, respectively.

Again, it is convenient to transform (16) into a standard eigenvalue problem as

$$\overline{\mathbf{Z}}_A^{-1} \cdot \overline{\mathbf{X}}_A \cdot \begin{bmatrix} ik\mathbf{J}_n \\ c\boldsymbol{\rho}_n \end{bmatrix} = (i - \lambda_n)^{-1} \begin{bmatrix} ik\mathbf{J}_n \\ c\boldsymbol{\rho}_n \end{bmatrix} \tag{19}$$

where the A-EFIE solution $\overline{\mathbf{Z}}_A^{-1} \cdot \mathbf{u}$ can be computed iteratively with a constraint preconditioning scheme. The same process is also applicable to (17).

V. FMA for CMA

In large-scale applications, characteristic modes of interest are normally solved for iteratively. ARPACK, based on the IRAM or the Lanczos variant for symmetric matrices, is appropriate for calculating a few eigenpairs of large sparse or structured matrices, where an MVP requires only $O(N)$ floating point operations [12]. However, when ARPACK is applied to dense eigenvalue problems, MVPs are challenged by the $O(N^2)$ complexity and storage requirement.

From (8), (14), and (19), the first type of required MVPs for constructing Arnoldi vectors are of forms $\overline{\mathbf{R}}_E \cdot \mathbf{u}$, $\overline{\mathbf{M}}_C \cdot \mathbf{u}$, and $\overline{\mathbf{X}}_A \cdot \mathbf{u}$ for EFIE-, CFIE-, and A-EFIE-based TCMs, respectively. The simplest approach to perform such MVPs is given by the following direct extraction.

Regarding an arbitrary vector $\mathbf{u}$, one can efficiently compute $\overline{\mathbf{Z}} \cdot \mathbf{u}$ with the conventional FMA, where $\overline{\mathbf{Z}} = \overline{\mathbf{R}} + i\overline{\mathbf{X}}$ is taken to be $\overline{\mathbf{Z}}_E$, $\overline{\mathbf{Z}}_H$, or $\overline{\mathbf{Z}}_A$. It is well known that midfrequency MLFMA reduces the computational complexity and memory cost of $\overline{\mathbf{Z}} \cdot \mathbf{u}$ to $O(N \log N)$, and the LF-FMA enables MVPs with an $O(N)$ complexity [18]–[20]. Hence, for an arbitrary complex vector $\mathbf{u} = \mathbf{u}' + i\mathbf{u}''$, providing that $\overline{\mathbf{R}}$ and $\overline{\mathbf{X}}$, $\mathbf{u}'$, and $\mathbf{u}''$ are all real, the required MVPs can be computed with a simple algebraic approach as

$$\begin{aligned} \overline{\mathbf{R}} \cdot \mathbf{u} &= \overline{\mathbf{R}} \cdot \mathbf{u}' + i\overline{\mathbf{R}} \cdot \mathbf{u}'' \\ &= \Re e\left[\overline{\mathbf{Z}} \cdot \mathbf{u}'\right] + i\Re e\left[\overline{\mathbf{Z}} \cdot \mathbf{u}''\right] \end{aligned} \tag{20}$$

and

$$\begin{aligned} \overline{\mathbf{X}} \cdot \mathbf{u} &= \overline{\mathbf{X}} \cdot \mathbf{u}' + i\overline{\mathbf{X}} \cdot \mathbf{u}'' \\ &= \Im m\left[\overline{\mathbf{Z}} \cdot \mathbf{u}'\right] + i\Im m\left[\overline{\mathbf{Z}} \cdot \mathbf{u}''\right] \end{aligned} \tag{21}$$

where $\Re e[\cdot]$ and $\Im m[\cdot]$ take the real and imaginary parts of the argument in the parentheses, respectively. Moreover, regarding the CFIE-based theory, $\overline{\mathbf{M}}_C \cdot \mathbf{u}$ is computed as

$$\begin{aligned} \overline{\mathbf{M}}_C \cdot \mathbf{u} &= \left[\alpha\overline{\mathbf{R}}_E + (1-\alpha)i\eta\overline{\mathbf{X}}_H\right] \cdot (\mathbf{u}' + i\mathbf{u}'') \\ &= \alpha\Re e\left[\overline{\mathbf{Z}}_E \cdot \mathbf{u}'\right] + i\alpha\Re e\left[\overline{\mathbf{Z}}_E \cdot \mathbf{u}''\right] \\ &\quad + (1-\alpha)i\eta\Im m\left[\overline{\mathbf{Z}}_H \cdot \mathbf{u}'\right] + (\alpha-1)\eta\Im m\left[\overline{\mathbf{Z}}_H \cdot \mathbf{u}''\right]. \end{aligned} \tag{22}$$

A more involved approach to compute $\overline{\mathbf{M}}_C \cdot \mathbf{u}$ adapts the plane-wave decomposition. Consider a spatial vector from the source point $\mathbf{r}_j$ in group m' to the observation point $\mathbf{r}_i$ in group m such that

$$\begin{aligned} \mathbf{r}_{ij} = \mathbf{r}_i - \mathbf{r}_j &= \mathbf{r}_i - \mathbf{r}_m + \mathbf{r}_m - \mathbf{r}_{m'} + \mathbf{r}_{m'} - \mathbf{r}_j \\ &= \mathbf{r}_{im} + \mathbf{r}_{mm'} + \mathbf{r}_{m'j} \end{aligned} \tag{23}$$

where $\mathbf{r}_m$ and $\mathbf{r}_{m'}$ represent the centers of groups m and m'. We can derive the following plane-wave decomposition:

$$\frac{\sin(kr_{ij})}{r_{ij}} = \int d^2\hat{k}\, e^{i\mathbf{k}\cdot(\mathbf{r}_{im}+\mathbf{r}_{m'j})}\, \alpha_{mm'}^{\Re}\left(\mathbf{k}, \mathbf{r}_{mm'}\right) \tag{24}$$

where

$$\alpha_{mm'}^{\Re}\left(\mathbf{k}, \mathbf{r}_{mm'}\right) = \frac{k}{4\pi}\sum_{l=0}^{L} i^l(2l+1)j_l(kr_{mm'})P_l\left(\hat{k} \cdot \hat{r}_{mm'}\right) \tag{25}$$

with L as the truncation number of an infinite series, $j_l(\cdot)$ as the spherical Bessel function of order l, and $P_l(\cdot)$ as the Legendre polynomial of degree l.

As there is no violation of addition theorem for (24), the FMM calculation may involve both the nearby and non-nearby groups of group m (except for itself), and the required MVPs in terms of a two-level algorithm are obtained as

$$\sum_{j=1}^{N}[M_C]_{ij}u_j = \sum_{j\in G_m}[M_C]_{ij}u_j + k\eta\int d^2\hat{k}\,\mathbf{V}_{fim}(\hat{k}) \cdot \sum_{m'\neq m}\alpha^{\Re}_{mm'}(\mathbf{k},\mathbf{r}_{mm'}) \cdot \sum_{j\in G_{m'}}\mathbf{V}_{sm'j}(\hat{k})u_j, \quad i\in G_m \tag{26}$$

where

$$\mathbf{V}_{sm'j}(\hat{k}) = \int_s d\mathbf{r}\left(\bar{\mathbf{I}}-\hat{k}\hat{k}\right)\cdot\mathbf{f}_j(\mathbf{r}_{m'j})e^{i\mathbf{k}\cdot\mathbf{r}_{m'j}} \tag{27}$$

and

$$\mathbf{V}_{fim}(\hat{k}) = \alpha\int_s d\mathbf{r}\left(\bar{\mathbf{I}}-\hat{k}\hat{k}\right)\cdot\mathbf{f}_i(\mathbf{r}_{im})e^{i\mathbf{k}\cdot\mathbf{r}_{im}} + (1-\alpha)\hat{k}\times\int_s d\mathbf{r}\,\hat{n}\times\mathbf{f}_i(\mathbf{r}_{im})e^{i\mathbf{k}\cdot\mathbf{r}_{im}}. \tag{28}$$

Regarding the multilevel algorithm, the standard MLFMA bookkeeping can still be employed for convenience [19]. However, a more efficient implementation conducts translation between nearby groups that belong to the same parent group at each level. Besides, the coarsest level is taken to be level-1 rather than level-2.

In addition, if MVPs such as $\overline{\mathbf{X}}_E\cdot\mathbf{u}$ and $\overline{\mathbf{R}}_H\cdot\mathbf{u}$ are to be computed, the following plane-wave decomposition can be used on condition that m and m' are not nearby groups or $|\mathbf{r}_{im}+\mathbf{r}_{m'j}|<|\mathbf{r}_{mm'}|$:

$$\frac{\cos(kr_{ij})}{r_{ij}} = \int d^2\hat{k}\,e^{i\mathbf{k}\cdot(\mathbf{r}_{im}+\mathbf{r}_{m'j})}\,\alpha^{\mathfrak{S}}_{mm'}(\mathbf{k},\mathbf{r}_{mm'}) \tag{29}$$

where

$$\alpha^{\mathfrak{S}}_{mm'}(\mathbf{k},\mathbf{r}_{mm'}) = \frac{-k}{4\pi}\sum_{l=0}^{L}i^l(2l+1)y_l(kr_{mm'})P_l\left(\hat{k}\cdot\hat{r}_{mm'}\right) \tag{30}$$

with the spherical Neumann function $y_l(\cdot)$ of order l.

Accordingly, the second type of required MVPs are $\overline{\mathbf{Z}}_E^{-1}\cdot\mathbf{u}$, $\overline{\mathbf{Z}}_C^{-1}\cdot\mathbf{u}$, and $\overline{\mathbf{Z}}_A^{-1}\cdot\mathbf{u}$, which are the solutions of EFIE, CFIE, and A-EFIE under arbitrary excitation vectors $\mathbf{u}$, respectively. As EFIE solutions $\overline{\mathbf{Z}}_E^{-1}\cdot\mathbf{u}$ are susceptible to the aforementioned difficulties, the conventional TCM has limited applications. However, we remedy the internal resonance problem with a CFIE-based TCM, where $\overline{\mathbf{Z}}_C^{-1}\cdot\mathbf{u}$ can be iteratively solved with Krylov subspace methods such as generalized minimal residual (GMRES) method and biconjugate gradient (BiCG) method. Sparse approximate inverse (SAI), incomplete LU preconditioning, and even Calderoén multiplicative preconditioning schemes can be employed to expedite the convergence of CFIE solutions [25]–[27]. If the computational time is taken prior to other factors, it is promising to decompose $\overline{\mathbf{Z}}_C$ beforehand by leveraging fast direct methods with adequate memory provided [28], [29]. On the other hand, we circumvent difficulties in multiscale modeling of small complex objects with the A-EFIE-based TCM. If $\overline{\mathbf{Z}}_A^{-1}\cdot\mathbf{u}$ is iteratively solved with a constraint preconditioning scheme, MVPs can be efficiently computed with the LF-FMA [10].

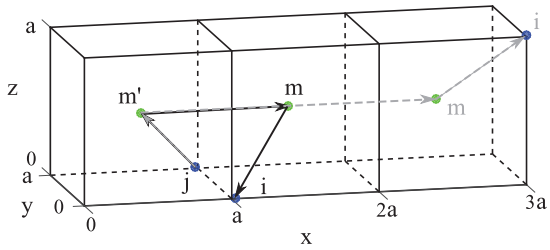

Fig. 1. Point positions.

VI. JDQZ for EFIE-Based TCM

It is of interest to point out that for EFIE-based TCM, when (7) is used to compute characteristic modes, IRAM may be a less appropriate choice if the decomposition of $\overline{\mathbf{X}}_E$ is not available. This is due to the lack of efficiency in solving $\overline{\mathbf{X}}_E^{-1}\cdot\mathbf{u}$ with conventional preconditioners, such as SAI. However, the generalized eigenvalue problem (6) can be solved with the Jacobi–Davidson QZ (JDQZ) method [14]. Without converting (6) to (7), the correction vector $\mathbf{t}$ can be obtained by approximately solving the Jacobi–Davidson correction equation

$$\left(\bar{\mathbf{I}}-\overline{\mathbf{R}}_E\cdot\mathbf{u}\cdot\mathbf{u}^*\right)\left(\overline{\mathbf{X}}_E-\sigma\overline{\mathbf{R}}_E\right)\left(\bar{\mathbf{I}}-\mathbf{u}\cdot\mathbf{u}^*\cdot\overline{\mathbf{R}}_E\right)\mathbf{t} = -\left(\overline{\mathbf{X}}_E-\sigma\overline{\mathbf{R}}_E\right)\mathbf{u}, \quad \mathbf{t}^*\cdot\overline{\mathbf{R}}_E\cdot\mathbf{u}=0 \tag{31}$$

where $\left(\sigma,\mathbf{u}=\overline{\mathbf{V}}\mathbf{s}\right)$ is a solution of

$$\overline{\mathbf{V}}^*\cdot\overline{\mathbf{X}}_E\cdot\overline{\mathbf{V}}\cdot\mathbf{s} = \sigma\overline{\mathbf{V}}^*\cdot\overline{\mathbf{R}}_E\cdot\overline{\mathbf{V}}\cdot\mathbf{s} = \sigma\mathbf{s} \tag{32}$$

with the search space $\overline{\mathbf{V}}$ containing several orthogonal basis with regard to $\overline{\mathbf{R}}_E$. The key is that even when (31) is solved with low accuracy, JDQZ still gives rise to correct solutions of (6). However, JDQZ becomes fairly slow in this case. Hence, it is also beneficial if efficient preconditioners are designed to accelerate the solutions of (31).

VII. Numerical Results

Numerical tests are first performed to validate the proposed plane-wave decompositions (24) and (29). We consider two cases as shown in Fig. 1, where the box size is a. In both cases, the source point j and source group center m' are located at $(0.9999a,\ 1.0a,\ 0.0)$ and $(0.5a,\ 0.5a,\ 0.5a)$, respectively. The observation point i and its group center m in Case 1 (dashed arrows) are located at $(2.9999a,\ 0.0,\ 1.0a)$ and $(2.5a,\ 0.5a,\ 0.5a)$, respectively, such that $|\mathbf{r}_{im}+\mathbf{r}_{m'j}|<$

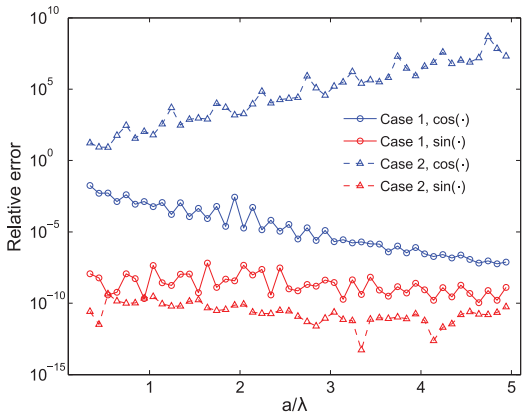

Fig. 2. Relative error of plane-wave decomposition for the real and imaginary parts of Green's function with respect to a/λ.

$|\mathbf{r}_{mm'}|$. The relative errors between left and right hand sides of (24) and (29) are calculated with respect to a/λ, where λ is the wavelength. The truncation number L is chosen to be

$$L \approx kd + 1.8 d_0^{2/3} (kd)^{1/3} \tag{33}$$

where the number of digits of accuracy d_0 is set to 3, and $d = \sqrt{3}a$ in this test. As shown in Fig. 2, excellent agreement is observed except for (29) or $\cos(\cdot)$ at lower frequencies ($a < 0.5\lambda$), which can be resolved with LF-FMA [20]. We then place the observation point i and its group center m at $(1.0001a,\ 0.0,\ 0.0)$ and $(1.5a,\ ;0.5a,\ 0.5a)$, respectively, in Case 2 (solid arrows) such that $|\mathbf{r}_{im} + \mathbf{r}_{m'j}| > |\mathbf{r}_{mm'}|$. As expected, (29) is no longer valid due to the violation of addition theorem. However, the regular part of the Green's function, i.e., $\sin(\cdot)$ can be computed with excellent accuracy (Fig. 2). This holds even when i and j are very close to each other. Although the results computed by (24) and (29) are not purely real, the imaginary parts are negligible as they are normally 10^{10} times smaller than the real parts.

The rest of numerical examples are computed with a non-parallel mixed-form FMA program on an Intel Core i5-2400 CPU with 3.10-GHz clock rate. Mixed-form FMA represents the field by multipoles for leafy levels in the quasi-static regime, and by plane waves for higher levels in the wave regime [10], [30]. In the rest of the examples, we use the plane-wave decomposition approach for the computation of $\overline{\mathbf{M}}_C \cdot \mathbf{u}$, and the direct algebraic approach for $\overline{\mathbf{X}}_A \cdot \mathbf{u}$. The open-source ARPACK package is employed as the iterative eigensolver unless specified otherwise. In this study, iterations in IRAM or JDQZ are referred to as outer iterations, and those in GMRES as inner iterations. Again, the free-space wavelength is denoted by λ.

A. Cuboid

We validate CFIE- and A-EFIE-based TCMs by computing characteristic modes of a perfectly conducting cuboid with a dimension of 1 m $\times$ 0.9 m $\times$ 0.3 m at 350 and 100 MHz, respectively. At 350 MHz, the triangular mesh comprises 1 280 patches and 1 920 edges, where the average edge length is around $0.08\,\lambda$. A few small characteristic values (CVs) are

TABLE I
CHARACTERISTIC VALUES (CVS) OF CUBOID COMPUTED BY EFIE AND CFIE AT 350 MHZ

CVs	EFIE	CFIE + FMA	Error (%)
$1 + i\lambda_1$	$1 + 0.3303i$	$1.0021 + 0.3310i$	0.21
$1 + i\lambda_2$	$1 + 0.3607i$	$1.0052 + 0.3563i$	0.64
$1 + i\lambda_3$	$1 - 0.3878i$	$1.0018 - 0.3861i$	0.23
$1 + i\lambda_4$	$1 + 0.4202i$	$1.0037 + 0.4174i$	0.43
$1 + i\lambda_5$	$1 + 0.5944i$	$1.0042 + 0.5921i$	0.41
$1 + i\lambda_6$	$1 - 0.6039i$	$1.0020 - 0.6007i$	0.32
$1 + i\lambda_7$	$1 + 0.6975i$	$1.0021 + 0.6993i$	0.23
$1 + i\lambda_8$	$1 - 0.7093i$	$1.0006 - 0.7040i$	0.44

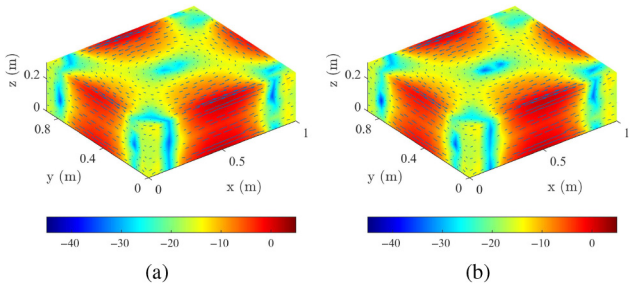

Fig. 3. Current patterns of mode $\mathbf{J}_1$ at 350 MHz computed by (a) EFIE and (b) CFIE (0.9) + FMA.

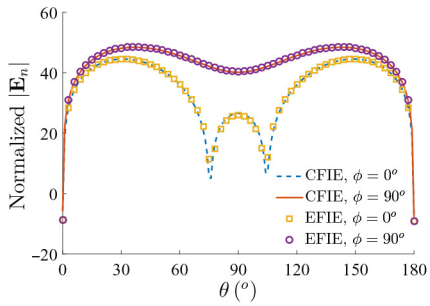

Fig. 4. Far-field pattern of cuboid mode $\mathbf{J}_1$ at 350 MHz.

computed with EFIE- and CFIE-based TCMs, namely (8) and (14), respectively, while FMA is only applied to CFIE of which the combination coefficient α is set to 0.9. The comparison is given in Table I, where good agreement is observed. Note that real parts of CVs resulted from CFIE are slightly different from 1. This is because, MFIE is not implemented to generate as accurate solutions as EFIE in this validation. On the other hand, EFIE- and CFIE-based TCMs yield the same characteristic modes. As an example, we plot in Fig. 3(a) and (b), the current patterns of $\mathbf{J}_1$ obtained by the two methods, respectively. A comparison of normalized far field patterns of this current is given in Fig. 4, where good agreement is observed. When the error tolerance of GMRES iterations is set to 10^{-4}, the average numbers of inner iterations in each outer one are around 600 and 70 for EFIE and CFIE, respectively, as a simple near-neighbor preconditioner is used.

To validate the A-EFIE-based TCM that addresses densely meshed objects that are not electrically large, we bring down the operating frequency to 100 MHz. To generate a reference, the

TABLE II
CHARACTERISTIC VALUES (CVS) OF CUBOID COMPUTED BY EFIE AND A-EFIE AT 100 MHZ

CVs	EFIE	A-EFIE + FMA	Error (%)
λ_1	0.5992	0.5959	0.55
λ_2	0.8960	0.8910	0.56
λ_3	−4.3001	−4.2893	0.25
λ_4	6.4258	6.4091	0.26
λ_5	−8.5905	−8.5718	0.22
λ_6	−8.6574	−8.6409	0.19
λ_7	10.6119	10.5448	0.63
λ_8	30.2488	30.2052	0.14

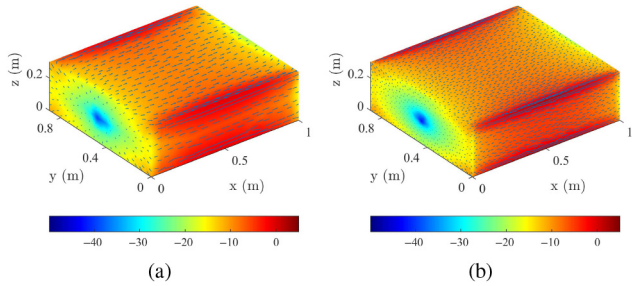

Fig. 5. Current patterns of mode $\mathbf{J}_1$ at 100 MHz computed by (a) EFIE and (b) A-EFIE + FMA.

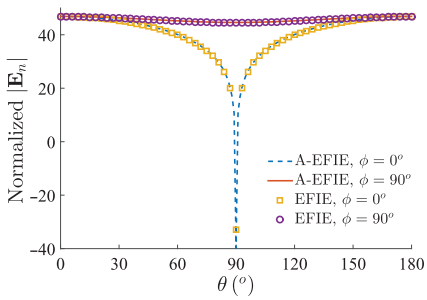

Fig. 6. Far-field pattern of cuboid mode $\mathbf{J}_1$ at 100 MHz.

original mesh is used with the EFIE-based formula (8) with an average edge length of $0.023\,\lambda$. A finer mesh containing 4 210 triangular patches and 6 315 inner edges is used with (19) based on A-EFIE, where the average edge length becomes $0.015\,\lambda$. As shown in Table II, characteristic values (CVs) obtained by EFIE agree well with those computed with A-EFIE and LF-FMA. We also find that characteristic currents generated by the two methods are consistent. For example, current patterns of $\mathbf{J}_1$ computed by EFIE and A-EFIE are plotted in Fig. 5(a) and (b), respectively. Their normalized far-field patterns are demonstrated in Fig. 6. A good agreement can be observed in both the current and far-field plots.

This example is also adopted to demonstrate the performance of JDQZ. In JDQZ, one can obtain correct characteristic values even with a small number of inner iterations (dimension of search space in GMRES), which indicates that (31) is only solved with poor accuracy each time. JDQZ and the original mesh are used to solve for five characteristic modes of the same

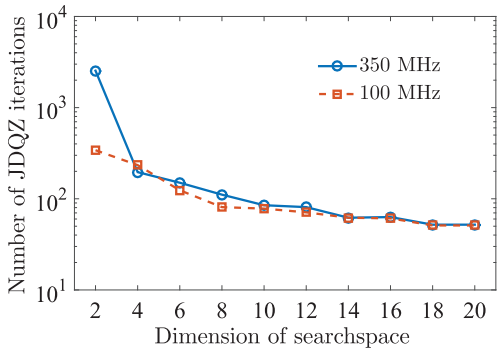

Fig. 7. Number of JDQZ iterations with respect to the dimension of GMRES searchspace.

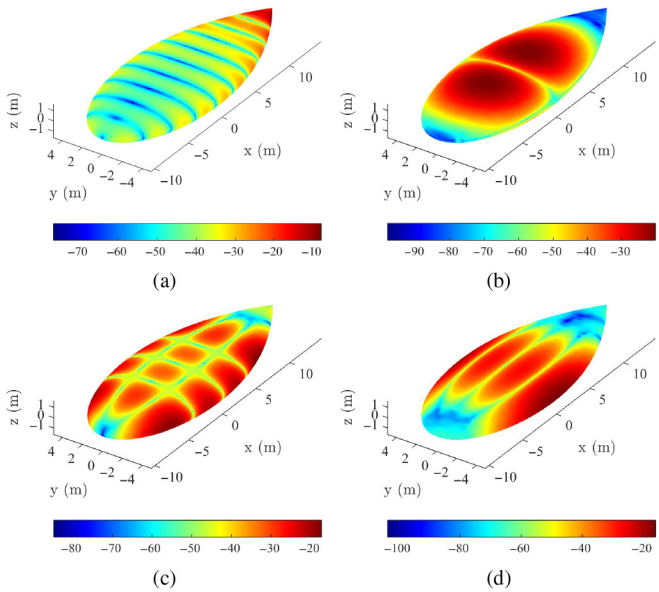

Fig. 8. Characteristic currents of a NASA almond. (a) $\mathbf{J}_1$. (b) $\mathbf{J}_2$. (c) $\mathbf{J}_3$. (d) $\mathbf{J}_4$. Their characteristic values are -0.0271, 0.0644, 0.0680, and 0.0768, respectively.

cuboid at 350 and 100 MHz, respectively. The convergence tolerance in JDQZ is set to 10^{-4}, which guarantees to generate correct characteristic modes. Fig. 7 shows the required number of outer (JDQZ) iterations with respect to the search space dimension of GMRES. Although a small search space reduces the computational time of each outer iteration, the tradeoff is that it increases the total number of outer iterations.

B. NASA Almond

We then consider a NASA almond that has a dimension of $5.05\,\lambda \times 1.95\,\lambda \times 0.65\,\lambda$ at 60 MHz. The mesh contains 36 090 triangular patches and 54 135 inner edges, and the average edge length is $0.0326\,\lambda$. To solve the CFIE-based eigenvalue problem (14), the CFIE combination coefficient is set to 0.5, and the GMRES error tolerance is set to 10^{-4}. The first four characteristic modes are computed by a six-level MLFMA using about 730-MB RAM, and their current patterns are plotted in Fig. 8. A typical convergence history of computing MVPs $\overline{\mathbf{Z}}_E^{-1} \cdot \mathbf{u}$ and $\overline{\mathbf{Z}}_C^{-1} \cdot \mathbf{u}$ with GMRES and near-neighbor preconditioning

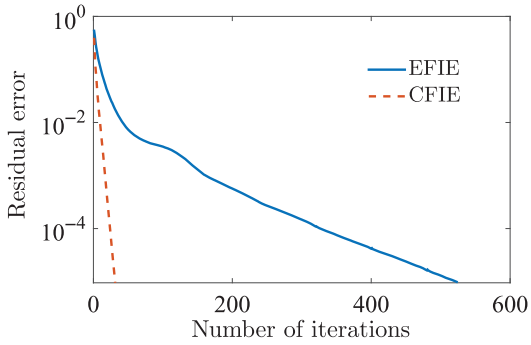

Fig. 9. Typical convergence history of inner (GMRES) iterations with EFIE and CFIE.

in an outer iteration is shown in Fig. 9, which clearly demonstrates the advantage of the proposed CMA. In [11], where a few modes of a vehicle ($0.5\,\lambda \times 0.23\,\lambda \times 0.25\,\lambda$) with 9 706 unknowns are computed with the EFIE-based formula (7), the memory usage is 3.54 and 2.8 GB for QZ factorization and IRAM, respectively. It is obvious that our scheme enables CMA of larger scale applications on a small computer.

Note that we herein are not considering extremely electrically large applications, because a great number of modes are needed for mode expansion, which renders CMA less useful. However, our method reserves the capability to address such challenging problems, provided that the direct decomposition of the full-rank matrix $\overline{\mathbf{Z}}_C$ is available.

C. Spiral Antenna

The next example is a spiral antenna with a dimension of $0.4\,\lambda \times 0.4\,\lambda \times 0.08\,\lambda$ at 1.64 GHz, where a dense mesh containing 60 552 triangular patches and 82 524 inner edges is used. The minimum, maximum, and average edge lengths are $0.169 \times 10^{-3}\,\lambda$, $0.733 \times 10^{-2}\,\lambda$, and $0.154 \times 10^{-2}\,\lambda$, respectively. The A-EFIE-based scheme is performed with a six-level LF-FMA, where the average number of GMRES iterations is 98 for the error tolerance of 1×10^{-4} with the usage of a constraint preconditioner. In this simulation, roughly 810-MB RAM is used to find five lowest modes. The current and radiation power patterns of a dipole mode, e.g., $\mathbf{J}_3$, and a quadrupole mode, e.g., $\mathbf{J}_4$, are plotted in Fig. 10(a)–(d), respectively. For comparison, we perform an EFIE-based CMA of the same antenna using a coarse mesh with 7 324 inner edges, where both matrices $\overline{\mathbf{R}}_E$ and $\overline{\mathbf{X}}_E$ are explicitly stored. When (7) is solved with the built-in MATLAB function *eigs* which implements IRAM, the memory usage is around 3.48 GB. A good agreement is observed between the characteristic values and normalized power patterns obtained by these two schemes, as shown in Table III and Fig. 11, respectively.

D. Package Board

In the last example, we consider a densely meshed model that is cut out of a realistic package board that contains two interconnect pairs. The triangular mesh has 79 480 patches and 114 240 inner edges, which leads to 193 719 unknowns

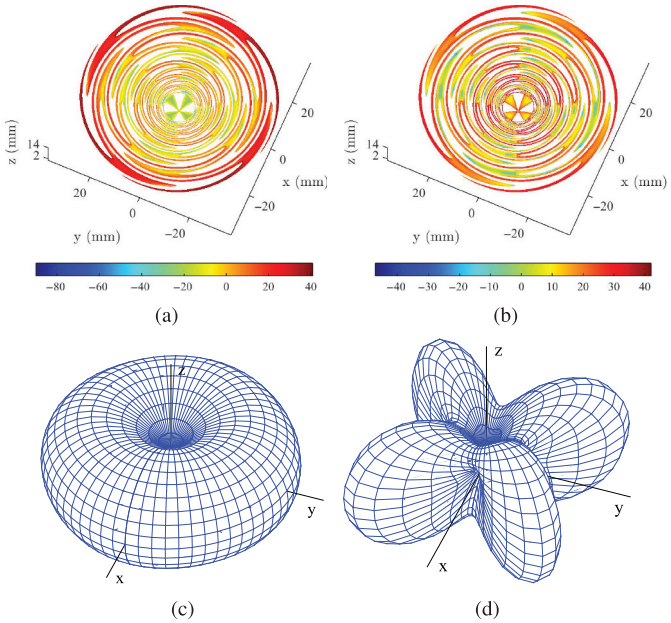

Fig. 10. Characteristic modes of a spiral antenna. (a) $\mathbf{J}_3$. (b) $\mathbf{J}_4$. (c) Power pattern of $\mathbf{J}_3$. (d) Power pattern of $\mathbf{J}_4$.

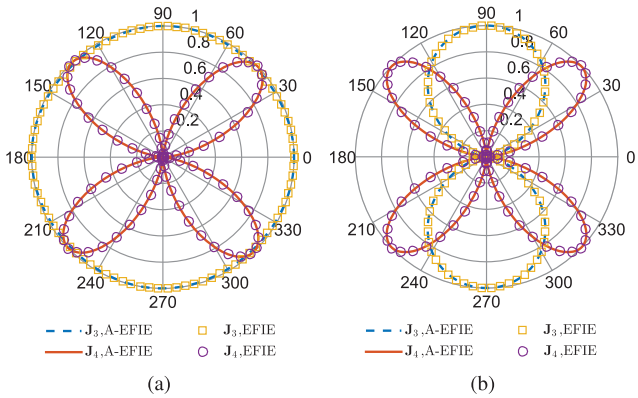

Fig. 11. Normalized power patterns of spiral antenna modes $\mathbf{J}_3$ and $\mathbf{J}_4$ computed by EFIE and A-EFIE at: (a) xy-plane ($\theta = 90°$) and (b) xz-plane ($\phi = 0°$).

TABLE III
CHARACTERISTIC VALUES OF SPIRAL ANTENNA COMPUTED BY EFIE AND A-EFIE AT 1.64 GHZ

CVs	EFIE	A-EFIE + LF-FMA	Error (%)
λ_1	2.1022	2.1511	2.33
λ_2	2.1022	2.1508	2.31
λ_3	−2.9582	−2.9739	0.53
λ_4	25.6066	25.5428	0.25
λ_5	53.7648	54.3620	1.11

in this simulation. The entire structure is around $0.2\,\lambda$ along the largest dimension at 3 GHz. The minimum, maximum, and average edge lengths are $0.454 \times 10^{-5}\,\lambda$, $0.368 \times 10^{-2}\,\lambda$, and $0.744 \times 10^{-3}\,\lambda$, respectively. The GMRES error tolerance is set to 0.15×10^{-4}, and on average, each outer iteration takes about 105 inner iterations for GMRES to converge as a constraint preconditioner is used. Totally, 120 (more than

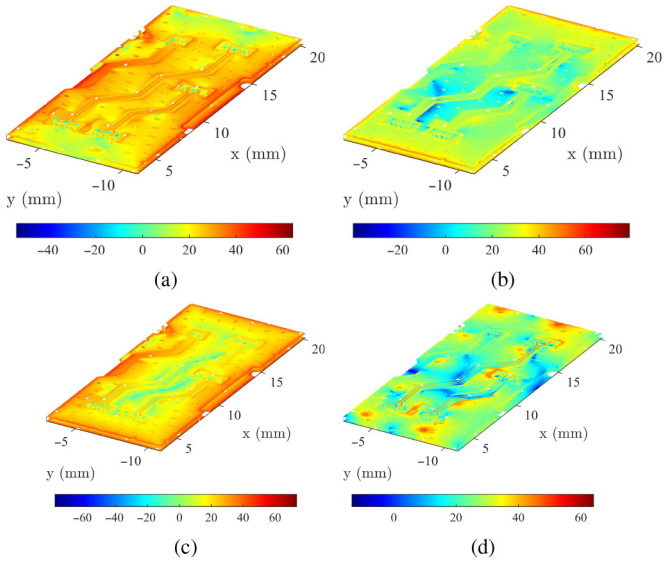

Fig. 12. Characteristic currents of a package board part. (a) $\mathbf{J}_1$. (b) $\mathbf{J}_2$. (c) $\mathbf{J}_3$. (d) $\mathbf{J}_4$. Their characteristic values are 19.5, 73.0, -121.0, and 1960.3, respectively.

enough) Arnoldi vectors are generated to compute four dominant characteristic modes. Their current patterns are illustrated in Fig. 12, where the characteristic values are also provided. The direct residuals of such eigensolutions are less than 10^{-3}. With the usage of a seven-level LF-FMA, the memory cost in this computation is less than 1 GB, and the CPU time is about 6 h.

VIII. Conclusion

In this article, we address large-scale CMA with FMAs. As the EFIE-based TCM is susceptible to the corruption of spurious internal resonances, we incorporate multilevel (ML-) FMA with a CFIE-based TCM to compute the modes of large closed conducting surfaces. The standard MLFMA program can be easily modified to perform the required matrix–vector multiplication operations in the iterative eigensolvers. On the other hand, an A-EFIE-based TCM is also developed for analyzing multiscale structures. By incorporating LF-FMA, it enables one to perform CMA for densely meshed objects that are not electrically large but contain fine components. Several numerical examples are provided to demonstrate the validity and efficiency of the proposed schemes. In even larger scale simulations, FMA can be implemented in parallel on many processors for better performance.

References

[1] R. J. Garbacz and R. H. Turpin, "A generalized expansion for radiated and scattered fields," *IEEE Trans. Antennas Propag.*, vol. AP-19, no. 3, pp. 348–358, May 1971.

[2] R. F. Harrington and J. R. Mautz, "Theory of characteristic modes for conducting bodies," *IEEE Trans. Antennas Propag.*, vol. AP-19, no. 5, pp. 622–628, Sep. 1971.

[3] R. F. Harrington and J. R. Mautz, "Computation of characteristic modes for conducting bodies," *IEEE Trans. Antennas Propag.*, vol. AP-19, no. 5, pp. 629–639, Sep. 1971.

[4] M. Cabedo-Fabrés, "Systematic design of antennas using the theory of characteristic modes," Ph.D. dissertation, School Telecommun. Eng., Univ. Politecnica de Valencia, Valencia, Spain, 2007.

[5] J. Ethier, "Antenna shape synthesis using characteristic mode concepts," Ph.D. dissertation, School Electr. Eng. Comput. Sci., Univ. Ottawa, Ottawa, ON, Canada, 2012.

[6] K. A. Obeidat, B. D. Raines, R. G. Rojas, and B. T. Strojny, "Design of frequency reconfigurable antennas using the theory of network characteristic modes," *IEEE Trans. Antennas Propag.*, vol. 58, no. 10, pp. 3106–3113, Oct. 2010.

[7] J. J. Adams and J. T. Bernhard, "A modal approach to tuning and bandwidth enhancement of an electrically small antenna," *IEEE Trans. Antennas Propag.*, vol. 59, no. 4, pp. 1085–1092, Apr. 2011.

[8] D. Manteuffel, "Characteristic modes–An intuitive approach for antenna design," in *Proc. IEEE Int. Conf. Comput. Electromagn.*, 2015, pp. 8–9.

[9] P. Yla-Oijala, M. Taskinen, and J. Seppo, "Analysis of surface integral equations in electromagnetic scattering and radiation problems," *Eng. Anal. Boundary Elem.*, vol. 32, pp. 196–209, 2008.

[10] Z. G. Qian and W. C. Chew, "Fast full-wave surface integral equation solver for multiscale structure modeling," *IEEE Trans. Antennas Propag.*, vol. 57, no. 11, pp. 3594–3601, Nov. 2009.

[11] D. J. Ludick, E. Lezar, and U. Jakobus, "Characteristic mode analysis of arbitrary electromagnetic structures using FEKO," in *Proc. Conf. Electromagn. Adv. Appl. (ICEAA)*, 2012, pp. 208–211.

[12] R. Lehoucq and D. Sorensen, "Deflation techniques for an implicitly restarted Arnoldi method," *SIAM J. Matrix Anal. Appl.*, vol. 17, no. 4, pp. 789–821, 1996.

[13] R. B. Lehoucq, D. C. Sorensen, and C. Yang, *ARPACK Users Guide: Solution of Large-Scale Eigenvalue Problems with Implicitly Restarted Arnoldi Methods*. Philadelphia, PA, USA: SIAM, 1998.

[14] D. R. Fokkema, G. L. G. Sleijpen, and H. A. van der Vorst, "Jacobi-Davidson style QR and QZ algorithms for the reduction of matrix pencils," *SIAM J. Sci. Comput.*, vol. 20, no. 1, pp. 94–125, 1998.

[15] L. Greengard and V. Rokhlin, "A fast algorithm for particle simulations," *J. Comput. Phys.*, vol. 73, pp. 325–348, 1987.

[16] R. Coifman, V. Rokhlin, and S. Wandzura, "The fast multipole method for the wave equation: A pedestrian prescription," *IEEE Antennas Propag. Mag.*, vol. 35, no. 3, pp. 7–12, Jun. 1993.

[17] J. M. Song and W. C. Chew, "Fast multipole method solution using parametric geometry," *Microw. Opt. Technol. Lett.*, vol. 7, pp. 760–765, 1994.

[18] J. M. Song, C. C. Lu, and W. C. Chew, "Multilevel fast multipole algorithm for electromagnetic scattering by large complex objects," *IEEE Trans. Antennas Propag.*, vol. 45, no. 10, pp. 1488–1493, Oct. 1997.

[19] W. C. Chew, J. M. Jin, E. Michielssen, and J. Song, *Fast and Efficient Algorithms in Computational Electromagnetics*. Norwood, MA, USA: Artech House, 2000.

[20] J. S. Zhao and W. C. Chew, "Three dimensional multilevel fast multipole algorithm from static to electrodynamic," *Microw. Opt. Technol. Lett.*, vol. 26, pp. 43–48, 2000.

[21] Q. I. Dai, Q. S. Liu, H. Gan, and W. C. Chew, "Combined field integral equation based theory of characteristic mode," *IEEE Trans. Antennas Propag.*, vol. 63, no. 9, pp. 3973–3981, Sep. 2015.

[22] A. Buffa and S. Christiansen, "A dual finite element complex on the barycentric refinement," *Math. Comput.*, vol. 40, pp. 1743–1769, 2007.

[23] Q. Chen and D. R. Wilton, "Electromagnetic scattering by threedimensional arbitrary complex material/conducting bodies," in *Proc. Antennas Propag. Soc. Int. Symp.*, 1990, vol. 2, pp. 590–593.

[24] K. Cools, F. P. Andriulli, F. Olyslager, and E. Michielssen, "Improving the MFIEs accuracy by using a mixed discretization," in *Proc. IEEE Antennas Propag. Symp.*, North Charleston, SC, USA, 2009.

[25] J. Lee, C. Zhang, and C. C. Lu, "Sparse inverse preconditioning of multilevel fast multipole algorithm for hybrid integral equations in electromagnetics," *IEEE Trans. Antennas Propag.*, vol. 52, no. 9, pp. 2277–2287, Sep. 2004.

[26] T. Malas and L. Gurel, "Incomplete LU preconditioning with the multilevel fast multipole algorithm for electromagnetic scattering," *SIAM J. Sci. Comput.*, vol. 29, pp. 1476–1494, 2007.

[27] H. Bağci, F. P. Andriulli, K. Cools, F. Olyslager, and E. Michielssen, "A Calderón multiplicative preconditioner for the combined field integral equation," *IEEE Trans. Antennas Propag.*, vol. 57, no. 10, pp. 3387–3392, Oct. 2009.

[28] J. Shaeffer, "Direct solve of electrically large integral equations for problem sizes to 1 m unknowns," *IEEE Trans. Antennas Propag.*, vol. 56, no. 8, pp. 2306–2313, Aug. 2008.

[29] H. Guo, J. Hu, and E. Michielssen, "On MLMDA/butterfly compressibility of inverse integral operators," *IEEE Antennas Wireless Propag. Lett.*, vol. 12, pp. 31–34, Mar. 2013.
[30] L. J. Jiang and W. C. Chew, "A mixed-form fast multipole algorithm," *IEEE Trans. Antennas Propag.*, vol. 53, no. 12, pp. 4145–4156, Dec. 2005.

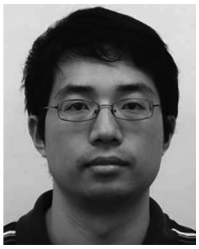

Qi I. Dai (M'14) received the B.S. degree in electronic engineering from the University of Electronic Science and Technology of China, Chengdu, China, in 2008, and the Ph.D. degree in electrical and electronic engineering from the University of Hong Kong, Pokfulam, Hong Kong, in 2014.

He is currently a Postdoctoral Research Associate with the Department of Electrical and Computer Engineering, University of Illinois at Urbana-Champaign, Champaign, IL, USA. He has been with the Center of Electromagnetics and Optics, University of Hong Kong, and the Center for Computational Electromagnetics and Electromagnetics Laboratory, University of Illinois at Urbana-Champaign, since 2009 and 2012, respectively. His research interests include developing electromagnetic numerical methods for modeling microwave-devices and Casimir forces, designing compact reverberation chambers, and applications of physics-based compressed sensing.

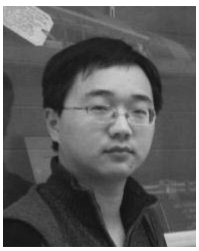

Junwei Wu was born in Henan, China. He received the B.S. degree from the ShanDong University, Jinan, China, in 2008, and the Ph.D. degree in radio physics from the WuHan Uinversity, WuHan, China, in 2015.

From 2012 to 2014, he was a Visiting Scholar at the University of Illinois at Urbana-Champaign, Urbana, IL, USA. His research interests include computational electromagnetics, radio-wave propagation, and array signal processing.

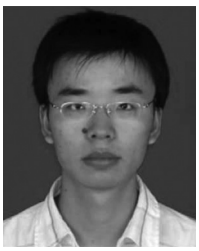

Hui Gan (S'14) received the B.S. degree in optics and the M.S. degree in electric engineering from Nanjing University of Science and Technology, Nanjing, China, in 2006 and 2008, respectively. He is currently working toward the Ph.D. degree in electric and computer engineering at the University of Illinois at Urbana-Champaign, Champaign, IL, USA.

His research interests include numerical methods and fast algorithms in computational electromagnetics.

Qin S. Liu (S'12) received the B.Eng. degree in electronic engineering from the University of Science and Technology of China (USTC), Hefei, China, in 2011. She is currently working toward the Ph.D. degree in electrical and electronic engineering at the University of Hong Kong, Pokfulam, Hong Kong.

Her research interests include numerical methods and fast algorithms in computational electromagnetics.

Weng Cho Chew (S'79–M'80–SM'86–F'93) received the B.S., M.S., Engineering, and Ph.D. degrees from the Massachusetts Institute of Technology, Cambridge, MA, USA, in 1976, 1978, 1978, and 1980, respectively, all in electrical engineering.

He served as the Cheng Tsang Man Visiting Professor with Nanyang Technological University, Singapore, in 2006, and the Dean of Engineering with the University of Hong Kong, Pokfulam, Hong Kong, from 2008 to 2011. He was a Professor and the Director of the Center for Computational Electromagnetics and the Electromagnetics Laboratory, University of Illinois at Urbana-Champaign, Champaign, IL, USA. Before joining the University of Illinois at Urbana-Champaign, he was the Department Manager and a Program Leader with Schlumberger-Doll Research, Cambridge, MA, USA. He was a Founder Professor with the College of Engineering, and previously, the First Y. T. Lo Endowed Chair Professor with the Department of Electrical and Computer Engineering, University of Illinois at Urbana-Champaign. From 2005 to 2007, he served as an IEEE Distinguished Lecturer. He is the Originator of several fast algorithms for solving electromagnetics scattering and inverse problems. He has authored a book entitled *Waves and Fields in Inhomogeneous Media* (IEEE Press, 1999), and coauthored two books entitled *Fast and Efficient Methods in Computational Electromagnetics* (Artech House, 2001), and *Integral Equation Methods for Electromagnetic and Elastic Waves* (1st edn., Morgan Claypool, 2007), authored or coauthored more than 300 journal publications, more than 400 conference publications, and more than 10 book chapters. His research interests include waves in inhomogeneous media for various sensing applications, integrated circuits, microstrip antenna applications, and fast algorithms for solving wave scattering and radiation problems.

Dr. Chew served on the IEEE Adcom for Antennas and Propagation Society as well as on the Geoscience and Remote Sensing Society. He has been active with various journals and societies. He is a Fellow of the Optical Society of America, Institute of Physics, Electromagnetics Academy, Hong Kong Institute of Engineers, and was the National Science Foundation Presidential Young Investigator. In 2002, the Institute for Science Information Citation elected him to the category of Most Highly Cited Authors (top 0.5%). He is the Editor-in-Chief of the *Journal of Electromagnetic Waves and Applications*/*Progress in Electromagnetic Research Journal*, and on the Board of Directors of Applied Science Technology Research Institute, Hong Kong. In 2008, he was elected by the IEEE AP Society to receive the Chen-To Tai Distinguished Educator Award. He was the recipient of the Schelkunoff Best Paper Award for the IEEE TRANSACTIONS ON ANTENNAS AND PROPAGATION, the IEEE Graduate Teaching Award, the UIUC CampusWide Teaching Award, and the IBM Faculty Awards.

Wei E. I. Sha (M'09) received the B.S. and Ph.D. degrees in electronic engineering at Anhui University, Hefei, China, in 2003 and 2008, respectively.

From July 2008 to May 2012, he was a Postdoctoral Research Fellow with the Department of Electrical and Electronic Engineering, University of Hong Kong, Pokfulam, Hong Kong, where he is currently a Research Assistant Professor. He has coauthored two books, respectively, on *Wavelet Theory* and *Finite-Difference Time-Domain Method*. He has authored 68 peer-reviewed journal papers included in Web of Science Core Collection. He also contributed to four book chapters at Springer, CRC Press, and InTech Publishers. He engages in theoretical and computational research in electromagnetics and optics, focused on the multiphysics and interdisciplinary research. The research topic is inspired by applications in several areas including solar energy, microwave/optical communication, sensing/detection, and quantum information. His research interests include fundamental and applied aspects in plasmonics, emerging photovoltaics, metasurfaces, quantum electrodynamics, and computational electromagnetics.

Dr. Sha is a member of OSA. He has served as a Committee Member or Session Chair of several international conferences including PIERS 2016, ICCEM 2016, IMWS-AMP 2015, EICT 2015, and ICSPS 2011. He has been serving as a Reviewer of IEEE, OSA, AIP, APS, and Nature Publishing Group journals. He received the Second Prize and First Prize of National Postgraduates Mathematical Contest in Modeling, respectively in 2006 and 2007. He was awarded Chinese Youth Science and Technology Innovation Prize in 2007. He and his collaborators received Research Output Prize at the University of Hong Kong in 2013. In 2015, he was awarded Second Prize of Natural Science from Anhui Province Government. He and his students received Second Place of Best Student Paper at PIERS 2014, First Place of Best Student Paper at ACES 2014, and Best Student Paper at NCMMW 2015. In 2014, he was awarded Outstanding Reviewer of *Journal of Computational Physics*.